Chemical zoning of garnets from the low-grade metamorphic rocks of the Silgara Formation, Santander Massif, Eastern Cordillera (Colombian Andes)

C. Rios and A. Takasu

Abstract

The Lower Paleozoic Silgara Formation is exposed in the Pescadero-Aratoca area, southwestern Santander Massif, and consists of metapelites and interlayered metabasic rocks intruded by Triassic-Jurassic calc-alkaline granites. A sequence of metamorphic zones was developed during Caledonian low-P/T metamorphism. The regional metamorphic grade of the Silgara Formation decreases southwestward, from the sillimanite zone, through the staurolite and garnet zones, to the biotite-zone. Metamorphism has occurred under conditions of high-temperature and low-pressure (Buchan type metamorphism), and reflects the high heat flow that exists in this part of the Santander Massif.

Garnet in the pelitic schists preserves chemical zoning, with decreasing X_{Mn}, and increasing X_{Fe} and X_{Mg} from core to rim, suggesting craystal growth during increasing temperature. X_{Ca} increases outwards and reaches a maximum at mantle, and is dependant on metamorphic pressure (maximum X_{Ca} indicates peak metamorphic pressure).

key words: chemical zoning; garnet; Silgara Formation; Santander Massif

INTRODUCTION

The low-P/T metamorphic rocks of the Silgara Formation, Pescadero-Aratoca area, southwestern Santander Massif, are intruded by Triassic and Jurassic igneous bodies (e.g. Goldsmith et al, 1971), see Fig. 1. In this area, metamorphic zonation from biotite to sillimanite zone developed at low pressure, and the metamorphic sequence ranges from the greenschist facies up to the upper amphibolite facies. Differing types of garnet zoning have been reported from the Sambagawa metamorphic belt in Japan: normal zoning (e.g. Banno et al, 1986; Takasu, 1984), reverse zoning (e.g. Itaya, 1978; Takasu, 1979, 1984; Higashino et al., 1981), resorption-overgrowth (e.g. Takasu, 1986; Takasu and Fujita, 1994) and sector zoning (e.g. Takasu and Kondo, 1993; Kitamura et al., 1993; Shirahata and Hirajima, 1995). In the study area, normal zoning and reverse zoning have been observed in garnet.

Metamorphic garnet in low-grade rocks often has distinct chemical zoning, and shows some of the greatest variability in terms of solid solution. Therefore, chemical zoning of garnet is of considerable value in the interpretation of metamorphic P-T history.

This paper describes the chemical composition and zoning of garnets within the metapelitic sequence of the Silgara Formation.

OCCURRENCE OF GARNET-BEARING SCHISTS

The Silgara Formation mainly consists of a metapelitic sequence, which displays a well-developed schistosity, although bedding (cross lamination) is well preserved locally. Lithology changes southwestward, from feldspathic psammitic schists to pelitic schists and more quartz-rich rocks, with zircon, apatite, tourmaline, graphite and Fe-Ti phases as the main accessory minerals. These rocks in general show a compositional banding of alternating muscovite-chlorite (and/or biotite)-rich bands and quartz-plagioclase-rich bands, and are characterized by the presence of garnet. (Fig. 2). A schistosity (S1) parallel to the compositional banding is defined by a preferred orientation of muscovite, chlorite and/or biotite, ilmenite and carbonaceous matter, which is usually affected by a crenulated schistosity (S2) defined by muscovite, biotite and/or chlorite, ilmenite and carbonaceous matter. A younger foliation (S3) is defined by the alignment of biotite.

Garnet zone. Garnet occurs as: (i) as small and euhedral grains (up to 0.1mm in diameter) which grew post-tectonically to S1 or S2. The grains are well preserved and contain abundant inclusions of ilmenite forming an internal foliation (S_{int}), which is concordant with the main fabric. (ii) large euhedral to subhedral garnet porphyroblasts (up to 4.5mm in diameter) that
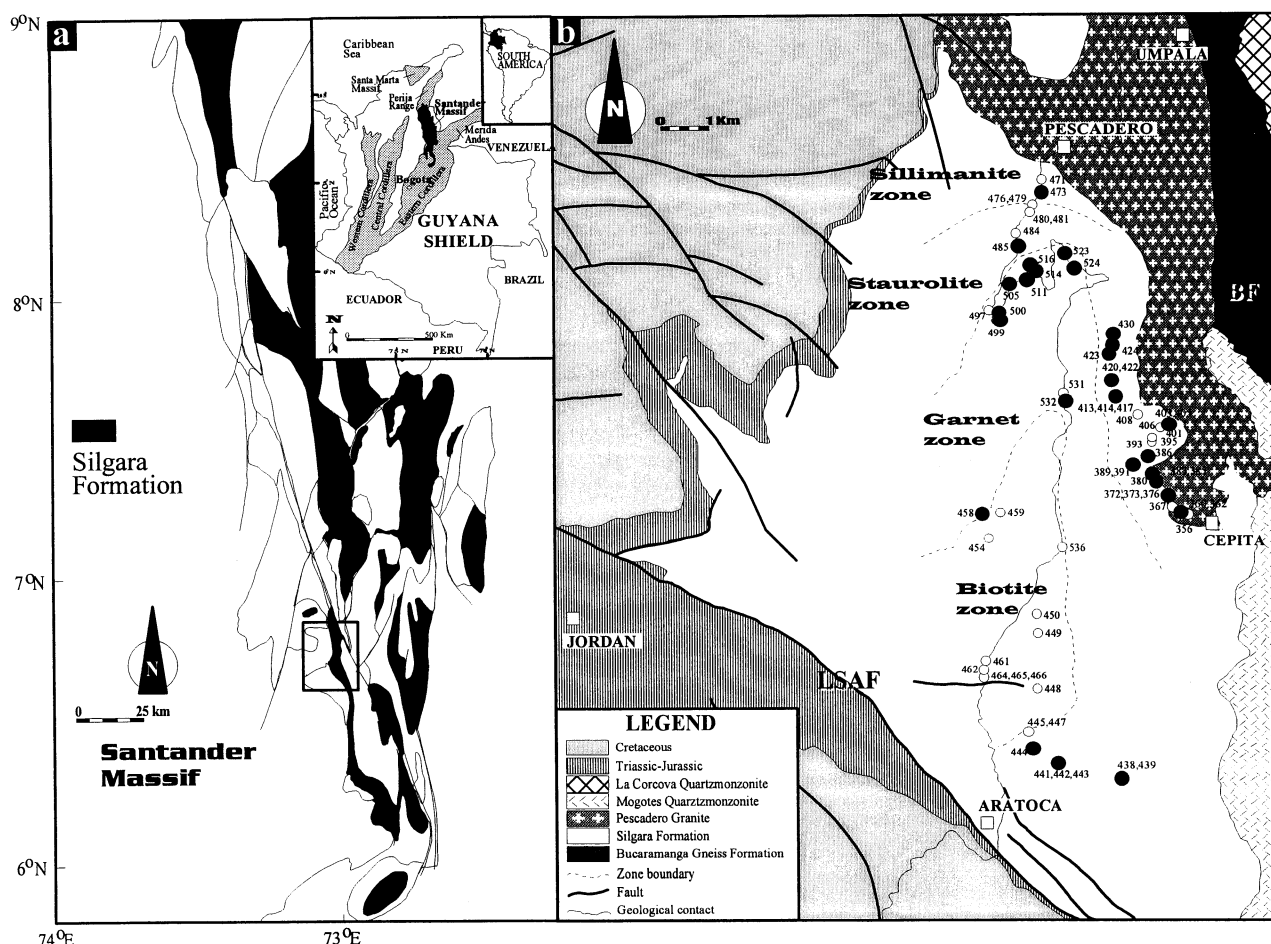
Fig. 1. Simplified geological map of the Pescadero-Aratoca area, southwestern Santander Massif (modified from Ward et al., 1973). Black dots show the distribution of garnet-bearing assemblages.

have muscovite, chlorite and ilmenite parallel to S2 wrapping around garnet. Garnet porphyroblasts sometimes contain inclusion trails of ilmenite and quartz, which define an internal foliation (S_{int}) that is rence: (i) discordant with the dominant schistosity (Fig. 2f).

Staurolite zone. Garnet shows two modes of occurrence: (i) as small and euhedral grains (up to 0.12mm in diameter) that grew post-tectonically to S1 or S2, and which contain ilmenite inclusions which are concordant with the main fabric (Fig. 2a): and (ii) as large porphyroblasts (up to 1.2cm in diameter), which show a pre-, syn- or post-tectonic character. Pre-tectonic garnet develops shattered, partially chloritized, porphyroblasts with pressure shadows and phyllosilicates and ilmenite laths lie parallel to S2 wrapping around garnet. Muscovite, biotite and quartz occur in strain shadows (Fig. 2c). Syn-tectonic garnet shows a

spiral structure, which has traditionally been interpreted as developing during syn-tectonic growth of rotating porphyroblasts during D2 (Fig. 2b). Post-tectonic garnet has overgrown to S1 or S2, with quartz and ilmenite as the main inclusions, concordant with the main fabric. Another characteristic texture occurring in post-tectonic garnet is that the fabric outside garnet porphyroblasts generally displays evidence of recrystallization and grain-size coarsening with respect to the inclusion-rich core in porphyroblasts (Fig. 2d). Garnet exhibits replacement by chlorite and epidote at rims and along cracks due to retrograde metamorphism (Fig. 2e), developing reaction rims mainly composed of chlorite, enclosing heavily corroded garnet cores.

Sillimanite zone. Garnet occurs as large and elongated subhedral to anhedral porphyroblasts (up to 3.5mm in diameter), which contain inclusions of quartz, biotite, muscovite and ilmenite, and appear to
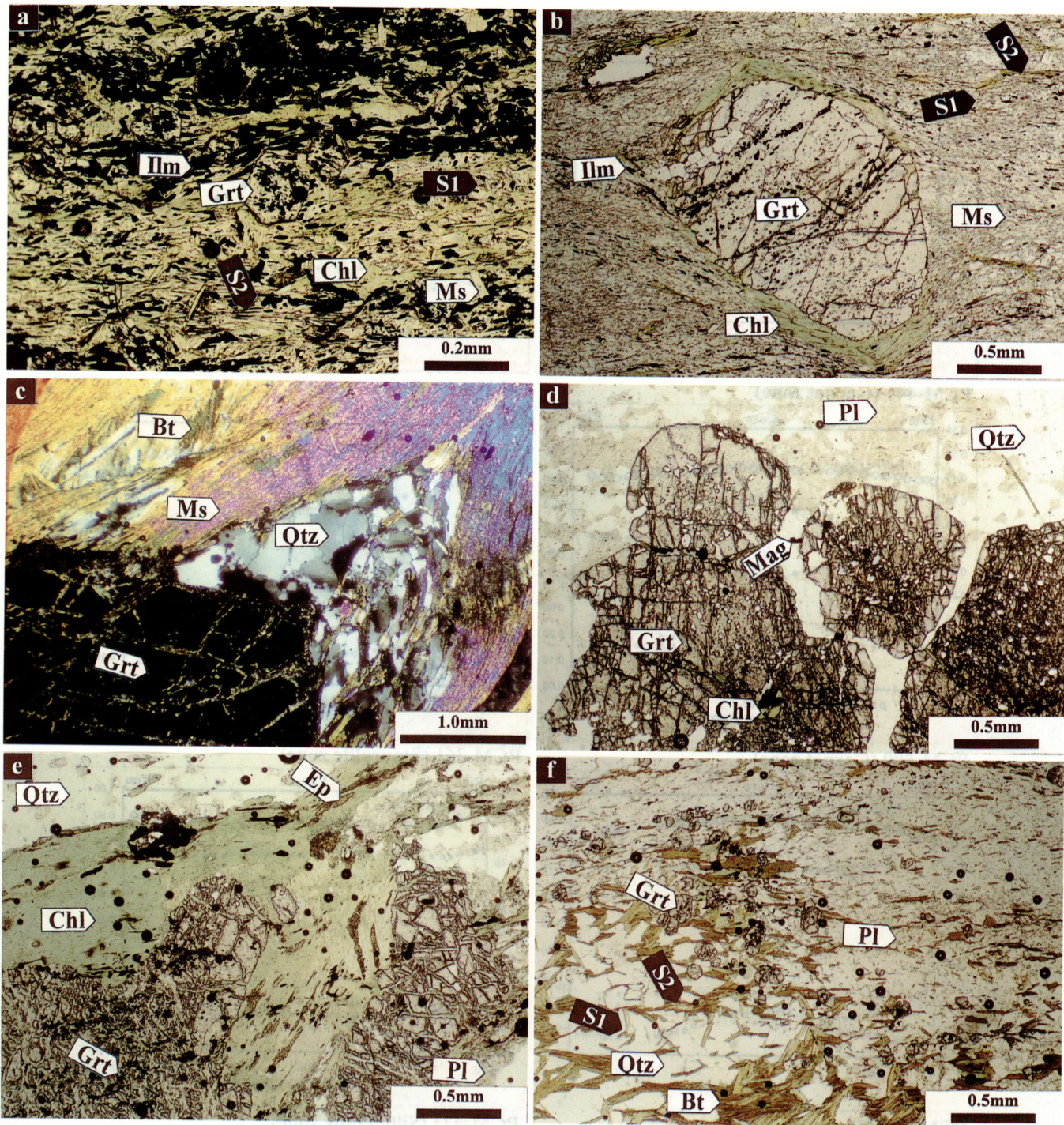
Figure 2. Occurences of garnet in metapelites of the Silgara Formation. (a) Small euhedral garnet porphyroblasts overgrowing a microcrenulated structure, suggesting a post-tectonic character. Opaque minerals occur as inclusions in garnet showing a S_{int} parallel to the S_{ext}. (b) Garnet partially chloritized is wrapped by the main schistosity (S2), which is folding a older schistosity (S1). (c) Garnet porphyroblast with pressure. (d) Large subhedral garnet porphyroblast consists of inclusion-rich core and inclusion-free rim (e) Garnet porphyroblast partly replaced by aggregate of chlorite and epidote. (f) Compositional banding of alternating biotite-rich layers and quartz-rich layers. A schistosity (S1) parallel to the compositional banding is affected by a crenulation with an axial plane cleavage (S2).
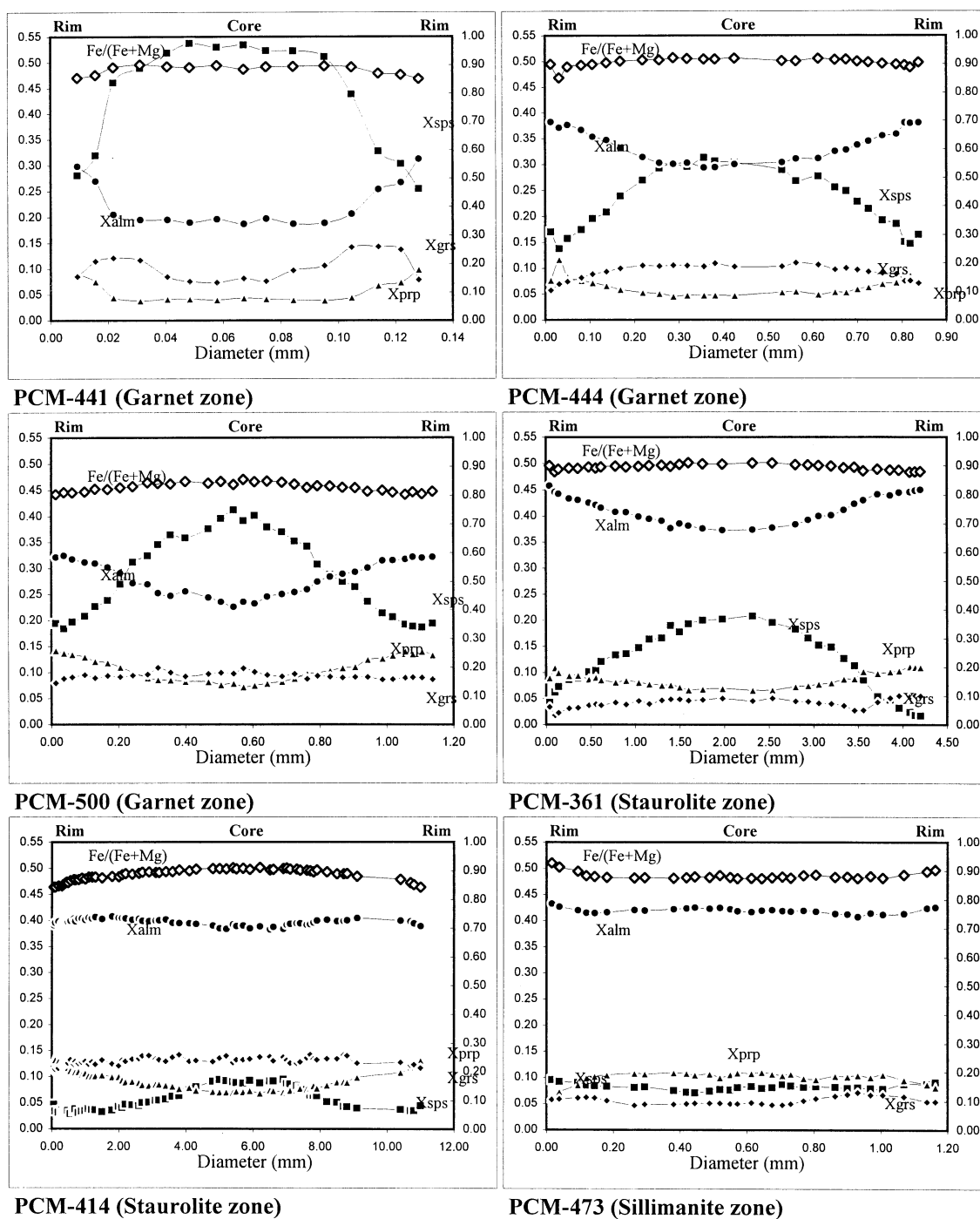
Fig. 3. Garnet zoning profiles in pelitic schists from the garnet, staurolite and sillimanite zones. Left axis for X_{sps}, X_{prp} and X_{grs}, and right axis for Fe/(Fe+Mg) and X_{alm}.

Fig. 4. Ternary plots of compositions of garnet in the garnet, staurolite and sillimanite zones expressed in (a) Mg-Mn-Fe and (b) Ca-Mn-(Fe+Mg) diagrams. Arrows in the upper right insets show compositional trends from core to rim.

Table 1. Representative chemical compositions of garnet from Silgara pelitic schists.

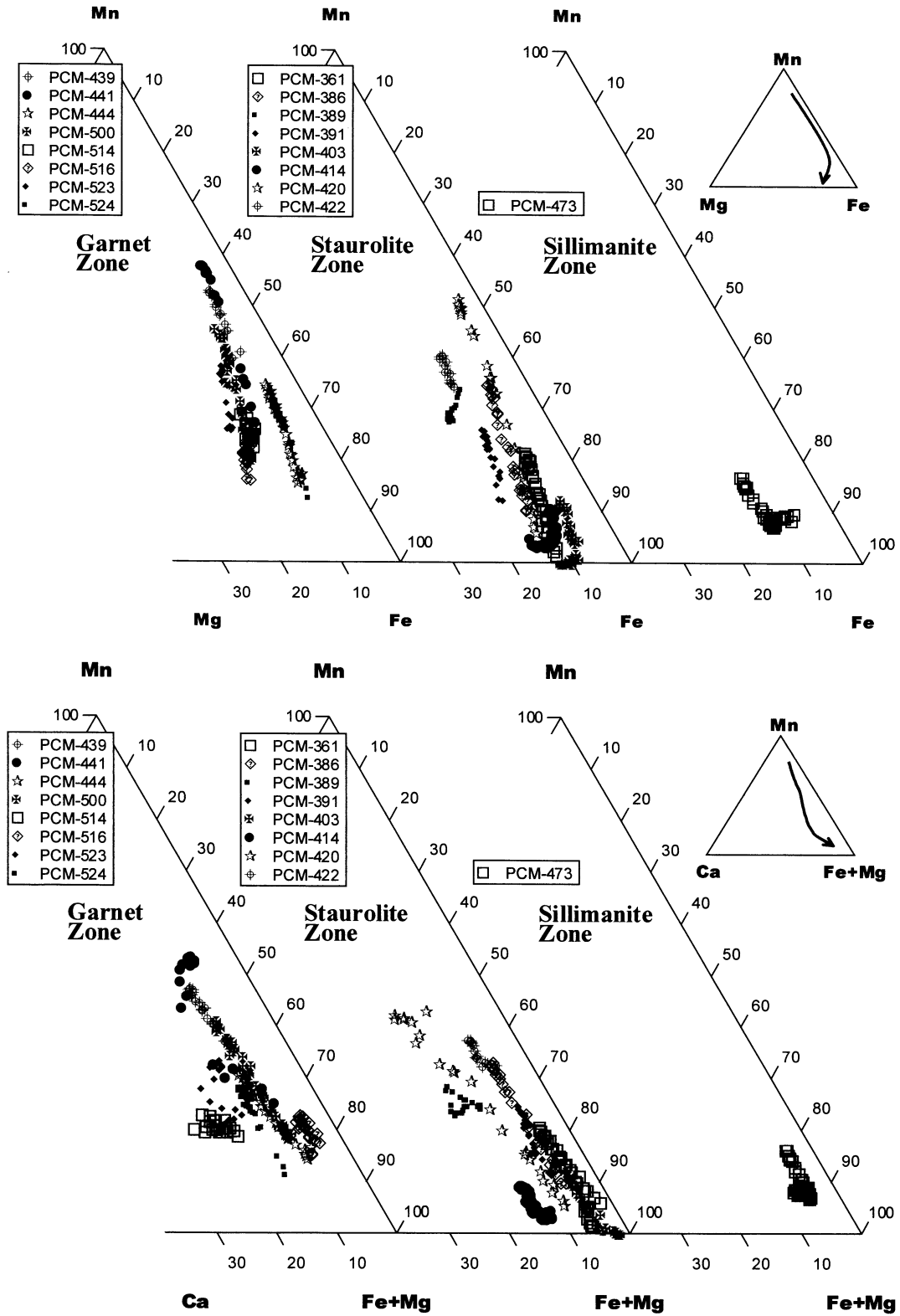| Sample	PCM-361		PCM-391		PCM-386		PCM-389		PCM-403		PCM-414		PCM-417		PCM-420		PCM-422		PCM-439		PCM-441		PCM-444		PCM-458		PCM-473	
Analysis	13	34	9	20	27	16	6	16	1	82	23	62	19	29	79	57	28	35	1	33	18	25	27	38	3	5	53	89
Weight %	rim	core	rim	core	rim	core	rim	core	rim	core	rim	core	rim	core	rim	core	rim	core	rim	core	rim	core	rim	core	rim	core	rim	core
SiO_2	37.73	36.79	37.14	37.78	37.66	36.99	38.14	37.19	37.39	36.86	37.31	36.49	37.55	36.84	37.19	36.78	37.50	36.46	37.34	38.30	36.39	36.50	37.58	37.14	36.81	36.45	36.53	37.00
TiO_2	0.00	0.12	0.06	0.10	0.01	0.12	0.00	0.06	0.05	0.00	0.04	0.03	0.03	0.03	0.07	0.04	0.26	0.16	0.07	0.24	0.02	0.05	0.00	0.10	0.08	0.09	0.03	0.00
Al_2O_3	20.61	20.55	20.50	20.93	20.56	20.08	21.22	20.16	21.05	20.69	20.42	19.96	20.53	20.04	20.78	20.60	21.64	20.35	20.37	23.46	20.64	20.29	21.14	20.54	20.30	19.88	20.12	20.34
FeO^*	38.36	32.10	28.33	27.11	31.88	24.04	21.69	22.21	40.06	35.36	32.26	31.37	29.05	18.83	31.80	17.84	22.86	20.37	21.13	14.63	25.42	16.63	31.13	24.43	27.94	24.72	35.81	31.16
MnO	1.91	9.21	7.03	9.72	5.86	14.42	11.83	12.83	0.13	5.29	2.06	4.03	6.68	18.36	4.25	18.67	14.66	16.43	16.06	17.64	12.28	23.43	7.53	13.84	9.97	14.01	3.81	7.26
MgO	2.29	1.68	3.15	3.07	2.50	1.48	3.20	2.55	2.59	1.39	3.30	1.81	2.72	0.99	2.62	0.91	3.00	2.60	1.88	1.04	2.26	1.09	1.94	1.20	2.02	1.18	1.98	2.75
CaO	1.21	1.61	2.88	2.32	2.07	2.16	5.22	5.75	0.90	1.69	3.88	4.61	3.34	5.23	2.72	4.22	2.09	2.85	3.41	3.41	2.95	2.84	2.01	3.63	2.45	2.65	2.31	1.57
Total	102.11	102.06	99.09	101.03	100.54	99.29	101.30	100.75	102.17	101.28	99.27	98.30	99.90	100.32	99.43	99.06	102.01	99.22	100.26	98.72	99.96	100.83	101.33	100.88	99.57	98.98	100.59	100.08
Cations per 12 Oxygens																												
Si	3.011	2.963	3.011	3.009	3.028	3.031	3.005	2.985	2.981	2.984	3.013	3.008	3.024	2.997	3.011	3.010	2.963	2.976	3.017	3.048	2.961	2.972	3.007	3.000	3.003	3.010	2.976	3.001
Ti	0.000	0.007	0.004	0.006	0.000	0.007	0.000	0.004	0.003	0.000	0.002	0.002	0.002	0.002	0.004	0.002	0.015	0.010	0.004	0.014	0.001	0.003	0.000	0.006	0.005	0.006	0.002	0.000
Al	1.939	1.951	1.958	1.965	1.948	1.938	1.970	1.907	1.978	1.974	1.943	1.939	1.948	1.921	1.982	1.987	2.015	1.958	1.940	2.200	1.979	1.947	1.993	1.955	1.952	1.935	1.932	1.944
Fe^{2+}	2.560	2.162	1.921	1.806	2.143	1.647	1.429	1.491	2.671	2.394	2.179	2.162	1.956	1.281	2.153	1.221	1.511	1.391	1.428	0.973	1.729	1.132	2.083	1.650	1.907	1.707	2.440	2.113
Mn	0.129	0.628	0.483	0.656	0.399	1.001	0.789	0.872	0.009	0.363	0.141	0.281	0.456	1.265	0.291	1.294	0.981	1.136	1.099	1.189	0.846	1.616	0.510	0.947	0.689	0.980	0.263	0.499
Mg	0.272	0.202	0.381	0.365	0.299	0.180	0.376	0.305	0.308	0.168	0.397	0.222	0.327	0.120	0.316	0.111	0.353	0.316	0.226	0.123	0.274	0.132	0.231	0.144	0.246	0.145	0.240	0.333
Ca	0.103	0.139	0.250	0.198	0.178	0.189	0.441	0.494	0.077	0.147	0.336	0.407	0.288	0.456	0.236	0.370	0.177	0.249	0.295	0.291	0.257	0.248	0.172	0.314	0.214	0.234	0.202	0.136
Total	8.014	8.052	8.008	8.005	7.995	7.993	8.010	8.058	8.027	8.030	8.011	8.021	8.001	8.042	7.993	7.995	8.015	8.036	8.009	7.838	8.047	8.050	7.996	8.016	8.016	8.017	8.055	8.026
X_{Fe}	0.90	0.91	0.83	0.83	0.88	0.90	0.79	0.83	0.90	0.93	0.85	0.91	0.86	0.91	0.87	0.92	0.81	0.81	0.86	0.89	0.86	0.90	0.90	0.92	0.89	0.92	0.91	0.86
X_{alm}	0.84	0.69	0.63	0.60	0.71	0.55	0.47	0.47	0.87	0.78	0.71	0.70	0.65	0.41	0.72	0.41	0.50	0.45	0.47	0.38	0.56	0.36	0.70	0.54	0.62	0.56	0.78	0.69
X_{sps}	0.04	0.20	0.16	0.22	0.13	0.33	0.26	0.28	0.00	0.12	0.05	0.09	0.15	0.41	0.10	0.43	0.32	0.37	0.36	0.46	0.27	0.52	0.17	0.31	0.23	0.32	0.08	0.16
X_{prp}	0.43	0.13	0.24	0.19	0.23	0.08	0.16	0.12	0.76	0.16	0.39	0.19	0.21	0.04	0.28	0.04	0.14	0.11	0.08	0.04	0.12	0.04	0.16	0.06	0.13	0.06	0.25	0.23
X_{grt}	0.03	0.04	0.08	0.07	0.06	0.06	0.15	0.16	0.03	0.05	0.11	0.13	0.10	0.15	0.08	0.12	0.06	0.08	0.10	0.11	0.08	0.08	0.06	0.10	0.07	0.08	0.06	0.04

*Total Fe as FeO. $X_{Fe} = Fe^{2+}/(Fe^{2+}+Mg)$, $X_{alm} = Fe^{2+}/(Fe^{2+}+Mn+Mg+Ca)$, $X_{sps} = Mn/(Fe^{2+}+Mn+Mg+Ca)$, $X_{prp} = Mg/(Fe^{2+}+Mn+Mg+Ca)$, $X_{grt} = Ca/(Fe^{2+}+Mn+Mg+Ca)$.

Sample	PCM-500		PCM-514		PCM-516		PCM-523		PCM-524		
Analysis	80	1	16	71	81	1	13	29	36	58	28
Weight %	core	rim	core	rim	core	rim	core	rim	core	rim	core
SiO_2	37.11	37.39	35.78	36.88	35.47	37.61	37.45	37.20	36.43	36.93	36.84
TiO_2	0.36	0.01	0.04	0.04	1.40	0.02	0.22	0.01	0.14	0.24	0.08
Al_2O_3	19.94	21.08	20.39	20.28	17.59	19.91	19.99	20.29	19.99	20.16	20.30
FeO^*	21.33	26.86	19.94	23.39	21.83	27.92	28.10	22.54	20.49	26.27	24.30
MnO	16.07	8.63	17.82	8.72	7.02	9.27	10.31	10.68	14.00	8.84	12.37
MgO	3.34	3.58	1.95	2.86	3.02	3.51	3.39	3.04	2.61	1.51	1.20
CaO	2.24	2.80	3.35	6.39	10.49	2.09	1.66	5.19	4.50	4.46	4.29
Total	100.39	100.35	99.27	98.56	96.82	100.33	101.12	98.95	98.16	98.41	99.38
Cations per 12 Oxygens											
Si	2.992	2.988	2.942	2.996	2.954	3.027	3.003	3.010	2.991	3.028	3.010
Ti	0.022	0.001	0.002	0.002	0.088	0.001	0.013	0.001	0.009	0.015	0.005
Al	1.895	1.985	1.976	1.941	1.727	1.888	1.889	1.935	1.934	1.948	1.955
Fe^{2+}	1.438	1.795	1.371	1.588	1.521	1.879	1.884	1.525	1.407	1.801	1.660
Mn	1.097	0.584	1.241	0.600	0.495	0.632	0.700	0.732	0.973	0.614	0.856
Mg	0.401	0.427	0.239	0.346	0.375	0.421	0.405	0.367	0.319	0.185	0.146
Ca	0.193	0.240	0.295	0.556	0.936	0.180	0.143	0.450	0.396	0.392	0.375
Total	8.038	8.020	8.066	8.029	8.096	8.028	8.037	8.020	8.029	7.983	8.007
X_{Fe}	0.78	0.81	0.85	0.82	0.80	0.82	0.82	0.81	0.82	0.91	0.92
X_{alm}	0.46	0.59	0.44	0.51	0.46	0.60	0.60	0.50	0.45	0.60	0.55
X_{sps}	0.35	0.19	0.39	0.19	0.15	0.20	0.22	0.24	0.31	0.21	0.28
X_{prp}	0.14	0.23	0.08	0.16	0.16	0.23	0.21	0.16	0.12	0.10	0.07
X_{grt}	0.06	0.08	0.09	0.18	0.28	0.06	0.05	0.15	0.13	0.13	0.12

be replaced by muscovite and sillimanite. Garnet commonly shows an skeletal and embayed character, with a concave contact with quartz or lesser plagioclase. Garnet shows replacement by chlorite at margins and along cracks, due to retrograde metamorphism. The dominant schistosity of the rock (S_{ext}), defined by muscovite, biotite and ilmenite, is broken by the presence of pre-tectonic garnet porphyroblasts.

CHEMISTRY OF GARNET

Chemical zoning of garnet in the Silgara pelitic schists has been investigated by electron microprobe analyses using a JEOL JXA 8800M electron probe microanalyzer in the Research Center for Coastal Lagoon Environments at Shimane University, with accelerating voltage and specimen current of 15kV and $2.0x10^{-8}$, respectively. Color map analysis: probe current $7.5x10^{-8}A$, dwell time 55 msec, no. of pixels 500x500, pixel size (mm) from 0.24x0.24 to 2.54x2.54. Garnet compositional zoning was documented not only with radial traverses of analytical points, with spacing of analytical points decreasing near the rim, but also with color map analyses and back-scattered electron imaging (BEI). Representative mineral compositions of garnet are given in Table 1.

Garnets in the Silgara pelitic schists generally exhibit chemical zoning of Fe, Mn, Mg and Ca, and are rich in almandine (X_{alm} = 0.34-0.88), with minor pyrope (X_{prp} = 0.03-0.28) and grossular (X_{grs} = 0.02-0.24) components. spessartine (X_{sps}) ranges from 0.00 to 0.54. Garnet zoning profiles show a "normal" zoning for Mn (bell-shaped X_{sps} profile). Mn decreases from core to rim (Fig. 3), whereas Fe and Mg increase. Garnet in calcic amphibole-bearing assemblages (e.g. sample PCM-514) is richer in grossular content (X_{grs} = 0.24) than that in calcic amphibole- free assemblages, suggesting that the former reflect more Ca-rich bulk compositions than do the latter. The compositional ranges encompassed by chemical zoning of garnet differ from rock to rock even at the same grade.

Core to rim trends in zoned garnets from the garnet, staurolite and sillimanite zones are shown in Mg-Mn-Fe and Ca-Mn-(Fe+Mg) triangular diagrams (Fig. 4). Garnets from pelitic schists of the Silgara Formation are divided into five types based on their chemical zonation (Figs. 3 and 4).

Type A shows a well-defined normal zoning, with increase in Mg and decrease in Mn and Ca from core to rim, with a small decrease in the Fe / (Fe+Mg) ratio (e.g. sample PCM-500).

Type B zonation tends to have a flattened slope, with a small increase in Mg and a small decrease in Mn and Ca from core to rim, with a slight decrease in the Fe / (Fe+Mg) ratio. After Mn content reaches a minimum, Fe / (Fe+Mg) ratio decreases with increasing Mn content (e.g. sample PCM-414).

Type C displays decrease in Mn content from core to rim, although the profile tends to be flattened in the central part. Ca content increases from core to mantle, and decreases from mantle to rim, with a small decrease in the Fe / (Fe+Mg) ratio (e.g. sample PCM-441).

Type D shows decreasing Mn from core to rim, although the profile tends to flatten in crystal interiors. Ca decreases outwards and reaches a minimum at the mantle, then increases towards the outermost rim, with a small decrease in Fe / (Fe+Mg) ratio (e.g. sample PCM-361).

Type E shows reversed zoning, with decrease in Mg and increase in Mn and Ca from core to rim, with a small increase in the Fe / (Fe+Mg) ratio (e.g. sample PCM-473). Note that profiles flatten in the interior of the crystal, and Ca content increases slightly from the outer core and reaches a maximum in the mantle.

Color maps of elemental distribution (Mg, Mn and Ca) for a type C garnet from a pelitic schist of the garnet zone (sample PCM-441) are given in Fig, 5. The relative concentration of each element is represented by color (see color bar). This shows distinct normal zoning, where MnO decreases and MgO increases from core to rim (spessartine content varies from 53.40 to 25.44 mol percent, and pyrope content varies from 4.36 to 9.89 mol percent). Ca is particularly interesting because it shows maximum content in the mantle of the crystal, and then decreases towards the rim, suggesting that peak pressure conditions were reached before peak temperature conditions. Fig. 3b shows the behavior of Ca content in the compositional trends of garnet from the differing metamorphic zones. There is little difference in the grossular contents, except in the mantle of some samples, as shown above. Fig. 6 shows color maps of elemental distribution within differing garnet types from the garnet, staurolite and sillimanite zones. These are discussed below.

ORIGIN OF THE CHEMICAL ZONING IN GARNET

There are two different styles of zoning pattern in garnet (Spear, 1993): (1) growth zoning occurs as successive shells of different composition are added to a growing crystal due to changes in external conditions (pressure-temperature or local bulk composition of the rock), and (2) diffusion zoning, in which a preexisting garnet is modified in composition by volume diffusion. In contrast to growth zoning, this requires no growth or consumption of the crystal. Whitney (1996) considers that in the growth and diffusion processes garnet (excluding the rim) is assumed to be a closed system with respect to the rock matrix. However, fractures allow the garnet to react with matrix phases, producing a significant change in the garnet composition, and therefore individual garnets may not be closed systems.

Chemical zoning in garnet from pelitic schist of the Silgara Formation shows a decrease in Mn content from core to rim, referred to as normal zoning, which is considered to be formed during prograde metamorphism. Such garnets seem unmodified by post-growth diffusion effects at the rim (e.g. PCM-441). We suggest that the rim compositions are most likely to represent peak metamorphic conditions and approach to equilibrium with coexisting phases.

Fig. 6a is a color map of the Ca distribution in a zoned type D garnet from the garnet zone. Note the concentric nature of the zoning, and how Ca reaches a minimum in the mantle, where an inclusion-rich core is surrounded by an inclusion-free rim. This reflects a decrease in pressure, and two stages of garnet growth.

Fig. 6b is a color map of Mn distribution in euhedral type A garnet, which seems unmodified by post-growth diffusion effects at the rim. Fig. 6c is a color map of Ca distribution in type D garnet. This shows differing zones of low Ca content, possibly reflecting decreases in pressure conditions during growth.
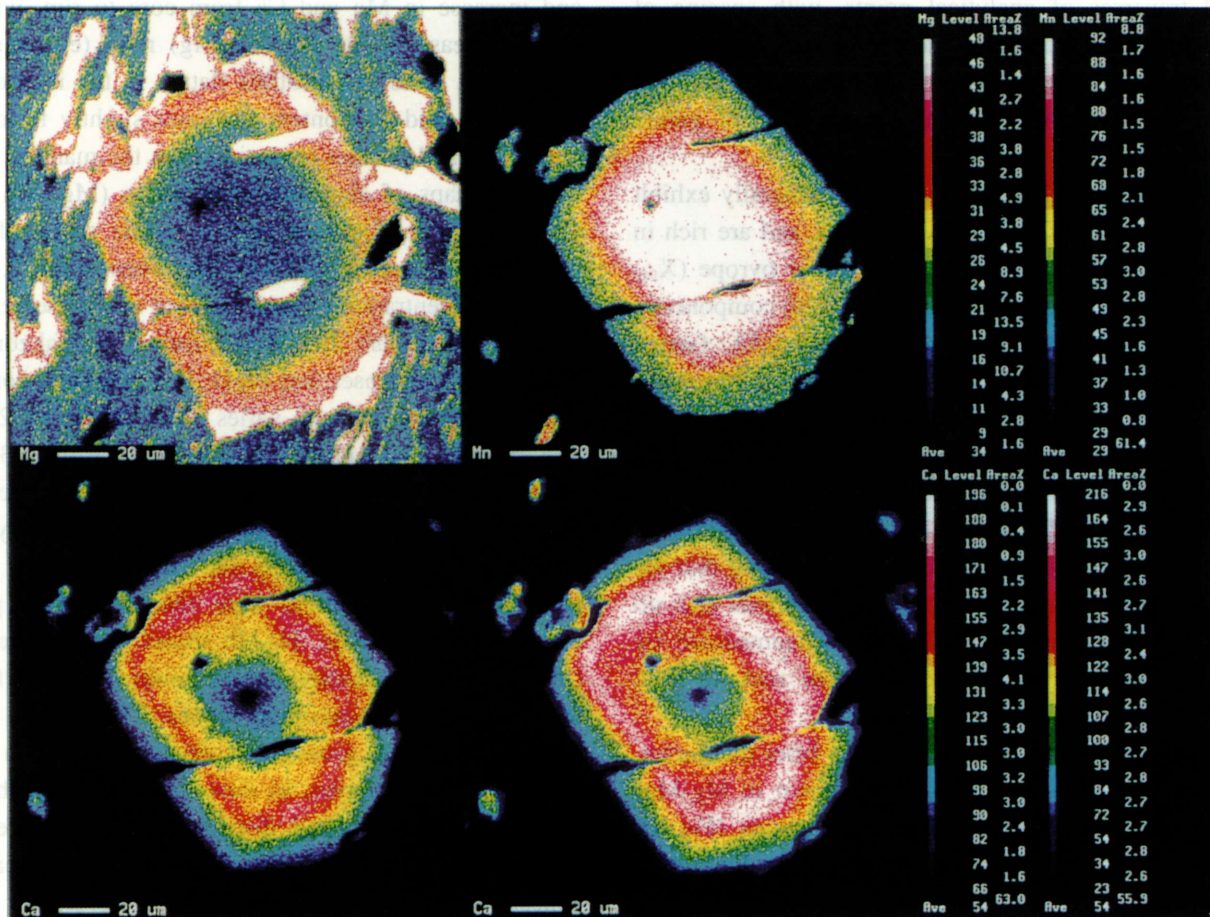
Fig. 5. Color maps showing element distributions (Mg, Mn and Ca) within type D garnet from the garnet zone of the Silgara Formation (sample PCM-441), Pescadero-Aratoca area, southwestern Santander Massif.
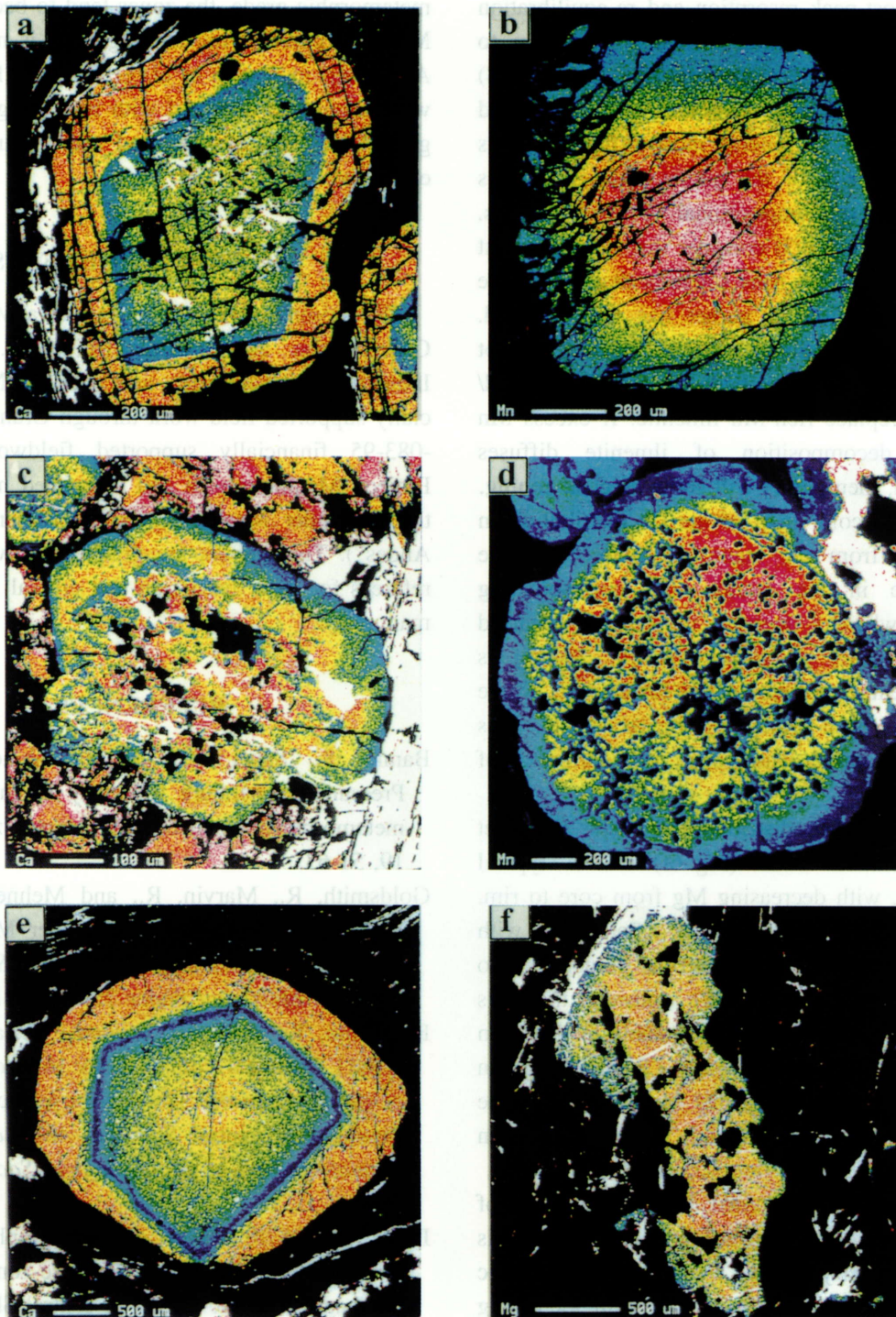
Fig. 6. Color maps showing elemental distributions within differing types of garnet from the metamorphic zones of the Silgara Formation. (a) Ca distribution in type D garnet (sample PCM-516, garnet zone), (b) Mn distribution in type A garnet (PCM-500, garnet zone), (c) Ca distribution in type D garnet (PCM-514, garnet zone), (d) Mn distribution in type A garnet from the staurolite zone (PCM-420), (Ca distribution in type D garnet, staurolite zone (PCM-361); (f) Mg distribution in type E garnet, sillimanite zone (PCM-473).

Fig. 6d shows that minimum Mn contents near rims also occur (e.g. sample PCM-420). This type of zoning is characterized as reversal zoning, which in many cases reflects post-peak resorption and re-equilibration during cooling, by elemental diffusion from rim to interior during retrograde metamorphism. Itaya (1978) described this type of reversed-zonation in garnet and discussed its genesis. In general, most diffusion effects will occur at the rim of the garnet, because this is where the steepest compositional gradient occurs. Whitney and Ghent (1993) consider that no significant increase in Mn at garnet rims suggests that major late metamorphic resorption of garnet has not occurred. However, a chloritization-resorption process cannot explain reversal zoning in euhedral garnet. Rutile and/ or sphene can replace rich-Mn ilmenite. If excess Mn liberated by decomposition of ilmenite diffuses towards the rim, then garnet will show reversal zoning.

Fig. 6 shows a color map of the Ca distribution in type D garnet from the staurolite zone. Note the euhedral shape in the mantle and corresponding minimum Ca, where a decrease in pressure occurred between two stages of garnet growth. Zoning is generally concentric, except in the lower part, where the zonation has been broken by the schistosity. This suggests that this garnet was broken after formation of the zones.

A color map of Mg distribution in type E garnet from the sillimanite zone (Fig. 6f) shows typical reversal zoning, with decreasing Mg from core to rim. Zonation becomes progressively flattened with increasing metamorphic grade from the garnet zone to the sillimanite zone (Fig. 3). We consider that this progressive homogenization is attributable to diffusion with increasing metamorphic grade. Such change in zoning character with increasing metamorphic grade from growth zoning to diffusion zoning has been reported by several studies (e.g. Tracy et al., 1976).

Banno et al. (1986) discussed the P-T trajectory of the Sambagawa prograde metamorphism on the basis of garnet chemistry, and established systematic changes in chemical zoning of garnet with increasing metamorphic grade. In the study area, no systematic changes in garnet composition occur with increasing metamorphic grade. Therefore, the differing patterns of chemical zoning observed are dependent on the bulk rock composition of the pelitic schists of the Silgara Formation. The most important features in Fig. 4 are: (1) rims become richer in Fe and Mg with increasing

metamorphic grade, (2) cores tend to decrease in Mn with increasing metamorphic grade, especially in staurolite-bearing assemblages, and (3) with increasing metamorphic grade, the zones tend to become richer in Mg from core to rim, although this is not systematic. According to Banno et al. (1986), the first feature is what should be expected with increasing metamorphic grade, but the second and third can not be so explained.

REFERENCES

Banno, S., Sakai, C., and Higashino, T. (1986) Pressure-Temperature trajectory of the Sambagawa metamorphism deduced from garnet zoning. *Lithos* 19, 51-63.

Goldsmith, R., Marvin, R., and Mehnert, H. (1971) Radiometric ages in the Santander Massif, Eastern Cordillera, Colombian Andes. *U.S. Geological Survey Professional Paper* 750-D, D41-D49.

Higashino, T., Sakai, C., Toriumi, M., and Banno, S. (1981) Chemical compositions and zonal structures of garnets from the Sambagawa pelitic schists in the Besshi area, central Shikoku. *Abstract of the 88th Annual Meeting of the Geological Society of Japan,* 385.

Itaya, T. (1978) Notes on petrography and rock-forming mineralogy (5) Reverse-zoned garnet in Sambagawa pelitic schists in central Shikoku, Japan. *J. Japan. Assoc. Min. Petr. Econ. Geol.* 73, 393-396.

Kitamura, M., Wallis, S., and Hirajima, T. (1993) Sector zoning and surface roughening of garnet in the Sambagawa metamorphic rock. *Proceedings 6th Topic. Meet. Crystal Growth Mechanism,* 215-220.

Shirahata, K., and Hirajima, T. (1995) Chemically sector-zoned garnet in Sambagawa schists, its mode

of occurrence and growth timing. *J. Japan. Assoc. Min. Petr. Econ. Geol.* 90, 69-79.

Spear, F.S. (1993) Metamorphic Phase Equilibria and Pressure-Temperature-Time Paths. Mineralogical Society of America, Washington, DC, 799pp.

Takasu, A. (1979) Basic intrusive rocks and metamorphism of the Sambagawa belt in the Besshi district, Shikoku. *Magma* 56, 8-14.

Takasu, A. (1984) Prograde and retrograde eclogites in the Sambagawa metamorphic belt, Besshi district, Japan. *Journal of Petrology* 25, 619-643.

Takasu, A. (1986) Resorption-overgrowth of garnet from Sambagawa pelitic schists in the contact aureole of the Sebadani metagabbro mass, Shikoku, Japan. *Journal of the Geological Society of Japan* 92, 781-792.

Takasu, A., and Kondo, Y. (1993) Color map photos of the Sambagawa garnets. *Earth Science* 47, 1-3.

Takasu, A., and Fujita Y. (1994) Resorption-overgrowth garnet from the Sambagawa pelitic schists in the Besshi district, central Shikoku, Japan. *Earth Science* 48, 8-13.

Tracy, R.J., Robinson, P., and Thompson, A.B. (1976) Garnet composition and zoning in the determination of temperature and pressure of metamorphism, central Massachusetts. *American Mineralogist* 61, 762-765.

Ward, D.E., Goldsmith, R., Cruz, B.J., Jaramillo, C.L., Restrepo, H. (1973) Geologia de los Cuadrangulos H-12, Bucaramanga y H-13, Pamplona, Departamento de Santander. *Boletin Geologico* XXI (1-3), 1-132.

Whitney, D.L. (1996) Garnets as open systems during regional metamorphism. *Geology* 24, 147-150.

(要　旨)

リオス　カルロス・高須　晃, 1999, コロンビア・アンデス, サンタンダー岩体のシルガラ変成岩中のざくろ石の累帯構造, 島根大学地球資源環境学研究報告, 18, 97-107

　　コロンビア・アンデス, サンタンダー岩体分布地域の南西部の Pescadero-Aratoca 地域の下部古生界シルガラ層は変成泥質岩とそれにはさまれる変成塩基性岩よりなる. これらの変成岩類はトリアス紀からジュラ紀の花こう岩によって貫入されている. カレドニア高温低圧型変成作用によりシルガラ層は変成作用を受け, その変成度はその分布の西南から北東へ, 黒雲母帯, ざくろ石帯, 十字石帯, 珪線石帯と変成度が上昇する.

　　ざくろ石帯より高温の変成岩では, 一般に泥質変成岩中のざくろ石は顕著な累帯構造を示し, その核部から縁部へ Mn は減少し, Fe と Mg は増加する. おそらくこれらのざくろ石は昇温変成作用によって形成された. また, Ca は核部から外側に向かって増加し, マントル部で極大値を示す. これらのざくろ石の化学組成累帯構造は, シルガラ変成岩の受けた変成作用の特徴を保存しているものと考えられる.